forum acusticum 2026
8-12 September · Graz, Austria

Numerical study on the effect of energy transfer from primary to secondary wave field with non-phase matched conditions

Christoph del Castillo Albildo[1], Benjamin Ankay[1], Daniel Pak[1], Chuanzeng Zhang[1]

[1]*Department of Civil Engineering, University of Siegen, Germany*

Abstract

The detection of localized material nonlinearities using guided waves is a valuable approach for nondestructive characterization and damage detection due to their ability to propagate over long distances and interrogate inaccessible domains. Of particular interest is the so-called wave mixing, in which the mutual interaction of two primary waves generates a secondary wave field. Phased-array scanning enables control of the location of the mixing-zone of the primary waves while the transmitters remain in a fixed position.

Aggravating damage detection, the amplitude of the resulting secondary wave is not invariably cumulative, especially when the group velocities differ and the mixing zones are finite. In addition to the secondary wave, changes in the primary waves, which may be attenuated or modified because of energy transfer to the secondary field, can be considered for the evaluation of measurements and the detection of nonlinearities.

This study numerically investigates how the energy transfer affects the amplitudes of propagating primary waves for the detection and assessment of a finite nonlinear material region in an otherwise linearly elastic plate. In addition a parametric study on the mixing-zone size and its influence is presented.

Keywords: n*onlinear ultrasonics, wave mixing, material characterization, nondestructive evaluation, phase matching condition*

1. Introduction

Structural Health Monitoring (SHM) and Non-Destructive Testing (NDT) play a crucial role across various engineering applications, as they enable the assessment of structural integrity without causing damage to the inspected component. Particularly in the context of aging infrastructure, these techniques provide a cost-effective solution by facilitating continuous monitoring, detecting early signs of deterioration, and thereby extending the service life of critical structures.

One of the most widely applied approaches is the detection of cracks or defects using ultrasonic waves. Measurement techniques such as the pulse-echo and pitch-catch methods are commonly employed for this purpose. Depending on the specific inspection method, access to both sides of the structure may also be required. In addition, the use of phased arrays and guided waves enables the inspection of a larger area without repositioning the probes [1]. All of these cases are generally based on the assumption of linear material behavior [2].

For conventional linear ultrasonic techniques, the resolution of material defects is strongly governed by the wavelength associated with the selected inspection frequency [3], [4], [5]. Consequently, the detection of micro-scale damages in practical applications suffers from fundamental physical limitations. In addition to these established conventional techniques, nonlinear ultrasonic methods have been developed. These methods exploit the nonlinear elastic properties of materials, enabling the detection of material changes that are well below the wavelength of the employed ultrasonic signals [4], [6]. As a result, nonlinear ultrasonic techniques exhibit higher sensitivity to early-stage micro-damages and offer a promising approach for the detailed investigation of the damage evolution in engineering structures under in-service loading conditions.

One approach is to detect higher harmonics, which are generated by the wave's self-interaction as it passes through a nonlinear material [7]. In addition, new secondary waves can be generated when two primary waves mix in a nonlinear material region [8]. By varying the mixing zone, damages or nonlinear regions can therefore not only be detected but also localized. However, the amplitude of the secondary wave is usually several orders of magnitude lower than that of

Corresponding author:
christoph.delCastilloAlbildo@uni-siegen.de

the primary wave, which makes measurements difficult. This study therefore investigates the energy transfer from the primary to the secondary wave field by analyzing the maximum amplitude of the primary wave in order to detect nonlinear regions of the material properties [9].

2. Theoretical Foundation

2.1 Wave motion in a nonlinear material

The theoretical foundation of nonlinear ultrasonic testing is based on the distortion of acoustic waves as they propagate through a nonlinear elastic medium. This wave distortion results from the self-interaction effects and leads to the generation of higher harmonic frequency components [10]. In the present study, only a material (physical) nonlinearity is considered.
For the propagation of an undamped one-dimensional (1D) longitudinal wave in an isotropic elastic material with a quadratic nonlinearity, the constitutive relationship is described by

$$\sigma = (\lambda + 2\mu)\left(\varepsilon + \frac{1}{2}\beta\varepsilon^2\right), \tag{1}$$

$$\beta = 2\frac{l + 2m}{\lambda + 2\mu}, \tag{2}$$

with the stress σ, the second-order elastic Lamé constants λ and μ, the third-order elastic constants l and m (Murnaghan notation), the nonlinearity parameter β (NLP), and the longitudinal modulus $(\lambda + 2\mu)$. The linear kinematic relation for the strain ε and the displacement u is given by

$$\varepsilon = \frac{\partial u}{\partial x}. \tag{3}$$

Substituting Eqs. (1) and (3) into the equation of motion $\partial\sigma/\partial x = \rho\, \partial^2 u/\partial t^2$, the following nonlinear equation of wave motion for the displacement can be established

$$\frac{\partial^2 u}{\partial t^2} = c_{\mathrm{L}}^2 \frac{\partial^2 u}{\partial x^2}\left(1 + \beta\frac{\partial u}{\partial x}\right), \tag{4}$$

with the longitudinal wave velocity

$$c_{\mathrm{L}} = \sqrt{\frac{\lambda + 2\mu}{\rho}} \tag{5}$$

and the mass density ρ.
For a time-harmonic excitation with an angular wave frequency of $\omega = 2\pi f$ (f is the wave frequency), a primary wave amplitude A_1, and a wavenumber of the propagating elastic wave k_{L}, the general solution of the corresponding partial differential Eq. (4) can be derived as [2]

$$u(x,t) = A_1 \sin(\omega t - k_{\mathrm{L}}x) + A_2 \cos(2(\omega t - k_{\mathrm{L}}x)). \tag{6}$$

The amplitude A_2 of the second harmonic depends on A_1, β, k_{L} and the position x. The NLP can therefore be expressed by the acoustic quantities as

$$\beta = \frac{8A_2}{k_{\mathrm{L}}^2 A_1^2 x}. \tag{7}$$

Consequently, valuable information regarding the material nonlinearity can be obtained by measuring the amplitude A_2 of the second harmonic component. Therefore, the second harmonic generation is a particularly promising approach for the damage detection and risk assessment, as the NLP β is for instance proportional to the micro-crack density [11], which can evolute, for example, as a result of the fatigue damage.
However, the amplitude of the second harmonic is typically several orders of magnitude lower than that of the fundamental wave, thus requiring highly sensitive measurement techniques. Furthermore, the measurement process is complicated by the fact that the signals of interest, which are usually located at twice the excitation frequency, can be affected and distorted by nonlinearities within the measurement system itself [8].

2.2 Wave propagation in elastic plates

Lamb wave propagation in an elastic plate is dispersive, meaning that the phase and group velocities of Lamb waves change depending on the wave frequency and plate thickness [12]. The waves investigated in this study are the fundamental symmetric Lamb wave S0 and the fundamental horizontal shear wave SH0. The particle displacement of the S0 mode is in the direction of the wave propagation, accompanied by a secondary contraction or expansion in the thickness direction symmetrical with respect to the mid-plane of the plate. For low frequency-thickness products (below 1 MHz · mm), the symmetric Lamb wave is slightly dispersive and represents the fastest-propagating wave mode in thin plates. Above 3 MHz · mm the phase velocity approaches that of the SH0 mode. The velocity of the SH0 wave is non-dispersive and the motion proceeds strictly parallel to the plate surface.

2.3 Mutual wave interaction

Korneev and Demčenko [13] described the nonlinear mutual interaction of two primary elastic waves in a solid, generating a secondary wave. For a secondary wave to form, the following two conditions for internal resonance must be met [14]:
1) Nonzero power flux
The sum of the nonlinear driving forces through the lateral boundaries f_n^{surf} and the volume f_n^{vol} must not be equal to zero, i.e.,

$$f_n^{surf} + f_n^{vol} \neq 0\,. \tag{8}$$

Otherwise, the secondary wave is not actually generated.

2) Phase matching condition (PMC)
Even though we are considering a nonlinear elastic medium, the resulting wave vector $\mathbf{k}_n$ must equal to the sum or the difference of the primary wave vectors $\mathbf{k}_a$ and $\mathbf{k}_b$, i. e.,

$$\mathbf{k}_n = \mathbf{k}_a \pm \mathbf{k}_b \,. \tag{9}$$

Based on these conditions, the phase velocity and frequency of the secondary wave can be calculated for two selected primary waves. The result must then be compared with the dispersion diagram to determine whether a suitable mode passes through the given point. Without discussing the details in depth, it should be noted here that the modes of the primary and secondary waves cannot be chosen arbitrarily. An overview of all possible mode combinations and a selected list of possible wave triplets can be found in [13] and [9].
In this study, the combination of two SH0 waves generating a S0 wave is considered. The phase velocity of the resulting wave is defined by

$$c_n = \frac{\omega_n}{k_n} = \frac{\omega_a \pm \omega_b}{\sqrt{k_a^2 + k_b^2 \pm 2k_a k_b \cos(\theta)}}, \tag{10}$$

with the wave numbers k and the angular frequencies ω of the primary waves (a, b) and the secondary wave (n) as well as the interaction angle θ between the primary waves. If the interaction angle is set to 0° the phase velocity of the secondary wave is equal to the primary waves. Because the SH0 mode is nondispersive, Eq. (10) yields a frequency-independent target phase velocity. The S0 mode itself is dispersive (see Figure 3), so exact phase matching occurs only at the frequency at which its dispersion curve reaches this velocity. A sample calculation is given in section 3. Due to the collinear wave propagation, it appears that, given the same frequency of the two primary waves, this is merely a case of self-interaction. However, since a new wave mode is generated, the term *mutual interaction* remains accurate. It is expected that the energy, flowing from the primary wave field to the secondary wave field via boundary and volume forces, in this interaction will lead to a decrease in the primary wave amplitude.

3. Numerical Study

3.1 FE models

A 1-mm-thick steel plate and a 1-mm-thick aluminum plate are considered as finite element (FE) models in the Solid Mechanics Modul of the FE Software COMSOL Multiphysics. The nonlinear material model is implemented as a hyperelastic material using the third order elastic (TOE) constants (Murnaghan notation) and Lamé constants as shown in Table 1. The TOE constants are later multiplied by a factor of 4 to simulate stronger material nonlinearities as they can occur in damaged regions [15].

Table 1. Lamé and Murnaghan constants of the material properties for steel and aluminum in [GPa].

Material	λ	μ	l	m	n
Steel	115.38	76.92	-300	-620	-720
Aluminum	55.27	25.95	-250	-330	-350

Brick elements with a fourth order shape function are used for the discretization of the domain. The maximum element size is set to half of the smallest wavelength which here corresponds to the sum of the excitation frequencies. The time-step is set to 1/40 of the smallest wave period. In both cases the sum of the excitation frequency is decisive. To reduce the computational time, a strip of one element width with periodic boundary conditions in the y-direction is modeled as shown in Figure 1. To excite the primary wave, a prescribed velocity is applied to the front surface which results in a displacement of 10 nm. The upper and lower side in the z-direction remain traction-free. The length of the model in the x-direction depends on the specific simulation time and is chosen to be large enough such that there is no interaction between the excitation side and the opposite side.

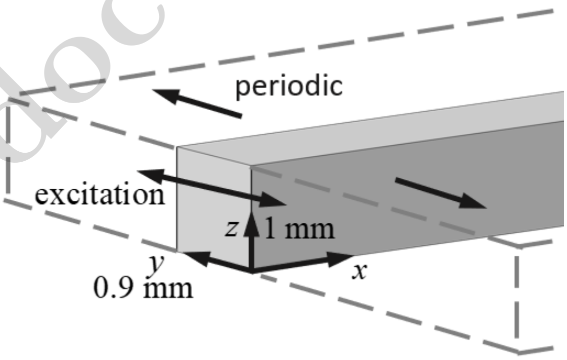

Figure 1. Finite section from a plate with an infinite dimension in the y-direction.

In addition to the entirely nonlinear model A, two strips with a finite nonlinear region of 100 mm are computed with the difference being where the region begins. In the model B the nonlinear region begins at $x = 0\,\text{mm}$, while in the model C it begins at $x = 100\,\text{mm}$.

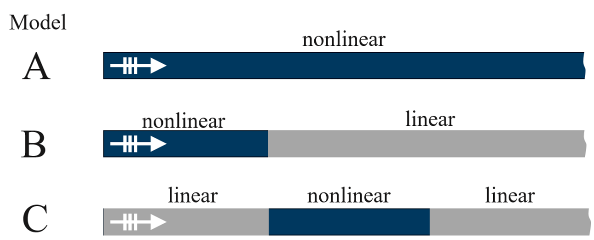

Figure 2. Overview of the model types with different nonlinear regions of the material properties.

3.2 Signal selection

As mentioned in the subsection 2.3, two SH0 waves are chosen as primary waves. Setting their frequencies equal results in a setup conducive to a later experimental verification, since only one actuator is needed. Although we focus on the amplitude of the primary waves in this study, it is worth noting that the secondary wave in this combination has an out-of-plane component, which should make it possible to detect it using an ultrasonic probe. The harmonic excitation signal is a Hann-windowed sine wave set to 9 cycles.

For two primary 1.65 MHz SH0 waves with a phase velocity of 3100 m/s we obtain the wavenumber 3445,1 m^{-1} and with Eq. (10) the phase velocity of 3100 m/s for the secondary wave. This corresponds well to the velocity of the S0 wave at 3.3 MHz, the sum of the excitation frequencies. Figure 3 shows the dispersion curves of the phase velocity, obtained by the *Dispersion Calculator v3.0*, and the calculated points for the secondary wave for a 1 mm aluminum plate.

The deviation from the frequency that satisfies the phase-matching condition is about 3, 9, and 15% for the aluminum plate model.

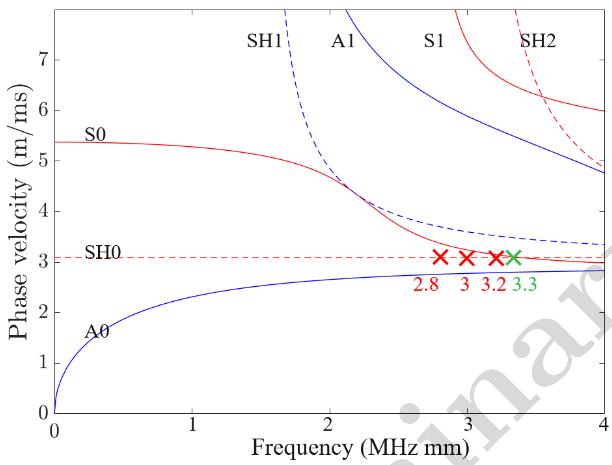

Figure 3. Phase velocity dispersion curves for the aluminum plate with marked phase matching frequency (green) and selected sum-frequencies of the study (red).

4. Numerical Results

4.1 Energy transfer indicated by decreasing primary wave amplitude

For the energy transfer evaluation, the maximum value of the primary wave displacement in the *y*-direction is plotted in Figure 4 for an infinite nonlinear elastic medium. It is clearly visible that as the deviation from the phase matching condition increases, the amplitude of the primary waves decreases less. To quantify this change, a linear slope is fitted to each dataset in the time range between 10 and 90 µs.

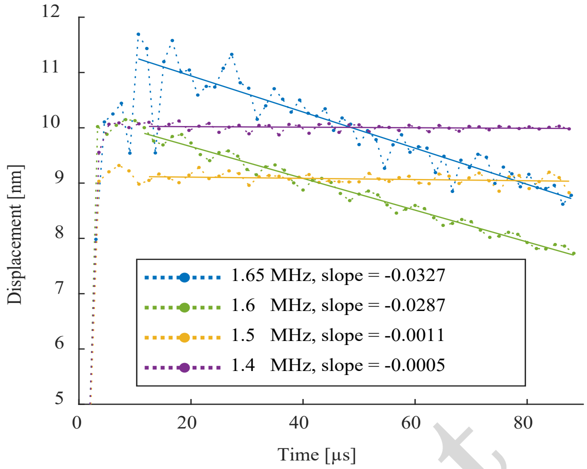

Figure 4. Maximum displacement in the *y*-direction and slope of the fitted line in [nm/µs] for the aluminum plate model (type A).

The same method is applied to the steel plate model and the slopes of the fitted lines for this model are listed in Table 2. The frequencies were adjusted to match the dispersion curve of the steel plate model. The phase matching condition is satisfied at a primary wave frequency of 1.7 MHz. In this case the deviation from the phase matching frequency is about 3, 6, and 12%. Since there are higher fluctuations in the displacement (Figure 5), particularly at the beginning, the linear fit was calculated using data from two different time periods.

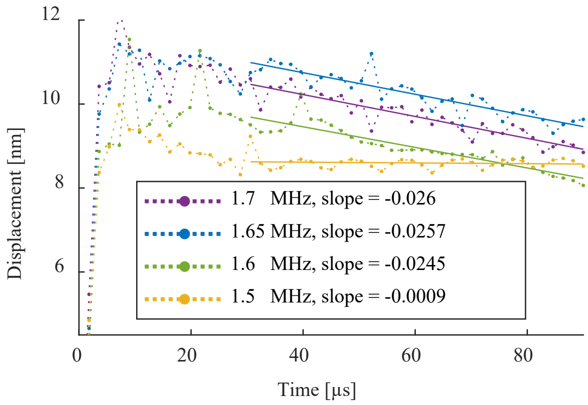

Figure 5. Maximum displacement in the *y*-direction and slope of the fitted line from 30 to 90 µs in [nm/µs] for the steel model (type A).

Table 2. Slopes of the fitted lines for the steel plate model (type A).

Frequency [MHz]	Slope 10 – 90 µs [nm/µs]	Slope 30 – 90 µs [nm/µs]
1.7	-0.0263	-0.0260
1.65	-0.0198	-0.0257
1.6	-0.0224	-0.0245
1.5	-0.0145	-0.0009

4.2 FFT analysis

To later assess the impact of the deviation from the phase matching condition, the fast Fourier transform (FFT) for each signal is calculated and presented in Figure 6, and the amplitude of half the ideal sum-frequency (1.65 MHz) is listed in Table 3.

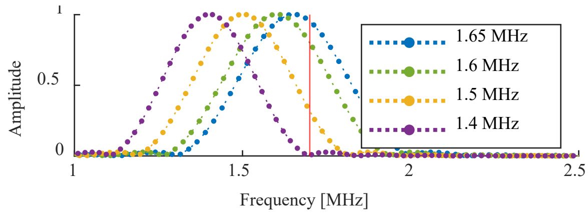

Figure 6. Normalized FFT of the excitation signals (aluminum plate) with vertical red line at 1.65 MHz.

Table 3. Normalized amplitude of the FFT at 1.65 MHz.

Frequency [MHz]	Normalized amplitude at 1.65 MHz
1.65	1
1.6	0.948
1.5	0.547
1.4	0.088

4.3 Effects of the nonlinear region

Figures 7 and 8 show the results of the models with varying sizes of the nonlinear material region for the steel plate model. For model type B the region always starts at the excitation surface (Figure 7), for model type C at a distance of 100 mm from it (Figure 8).
As already seen in the model type A, the results for the aluminum plate appear comparable for the other two models (types B and C) as well and show the same trend.

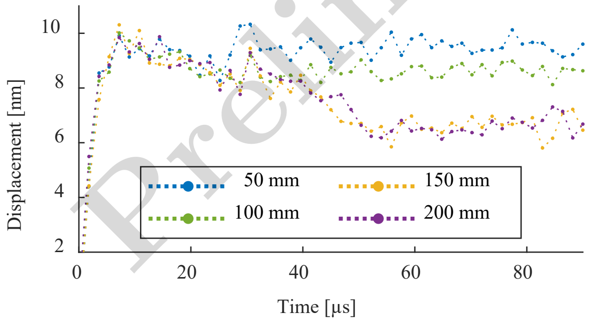

Figure 7. Maximum displacement in the y-direction for model type B (steel) with different lengths of the nonlinear region.

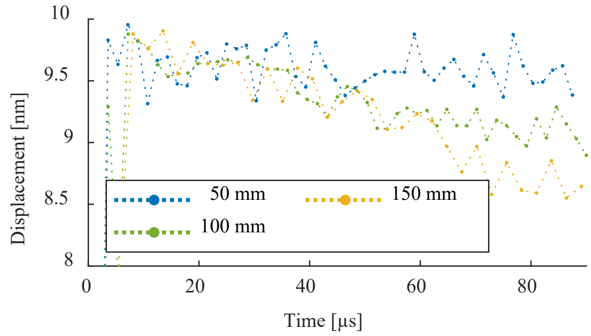

Figure 8. Maximum displacement in the y-direction for model type C (steel) with different lengths of the nonlinear region.

5. Discussions

The nonzero power flux transfers energy from the primary to the secondary wave field. This results in a decrease of the primary wave amplitudes which can be seen in Figures 4, 5, 7 and 8 for both infinite and finite nonlinear material regions respectively. It is clearly evident that even at a deviation of 9%, there is no longer any noticeable decrease in the wave amplitude since the slope of the fitted line is nearly zero (Figure 4). Signals with more cycles than those used in this study are likely to amplify this effect, as the peak in the FFT becomes narrower and the proportion of the optimal frequency thus decreases. Conversely, it can be assumed that a smaller number of cycles results in a broader frequency spectrum and thus a larger proportion of the frequency that satisfies the phase-match condition.
The different levels to which the signals initially rise (Figure 4) are likely due to the excitation at a prescribed velocity, which results in varying displacement magnitudes depending on the frequency.
The difference in the nonlinear region size is evident in all models based on the amplitude of the primary waves. For the steel plate, a gradual decrease can be observed in Figure 7 for lengths between 50 and 150 mm before the amplitude stabilizes at a certain level. This is consistent with the assumption that the reason for this is the generation of the S0 wave, which occurs only in the nonlinear region. Between 150 and 200 mm, no significant difference can be observed. This is also supported by the results from the model type C (Figure 8), in which the decrease does not begin until the wave reaches the nonlinear region and varies in magnitude depending on the size of that region. As expected, the displacement amplitudes in model types B and C for the aluminum and steel plates are qualitatively similar. The reason for the variation in the individual data lines could result from the interference of the primary waves with the second harmonic, which generates from the self-interaction within the nonlinear material. Since this wave mode is non-dispersive, it has the same group velocity as the primary waves. This is also supported by the observation that the variation is

periodic, as best seen in Figure 4 (1.4-1.6 MHz) for the aluminum plate and in Figure 5 (1.5 MHz) for the steel plate.

6. Conclusions

In this study, we investigate the decrease in the amplitude of the primary waves resulting from the energy transfer to the secondary wave and we have shown that the size of the nonlinear region has a significant influence on this. We are able to demonstrate that the effect is still visible even when the excitation frequency deviates from the phase-match condition by 3%. Noticeably, in the aluminum plate there is an abrupt change in the slope between 1.6 and 1.5 MHz. Although the FFT analysis confirms a significant reduction in the phase matching frequency component, an investigation using finer steps would still be informative.

The results provide a guidance on the basic conditions for experimental studies but have yet to be validated. In addition, further investigation on the effects of the number of excitation cycles would also be helpful in order to quantify its influence.

References

[1] P. Cawley, "Guided waves in long range nondestructive testing and structural health monitoring: Principles, history of applications and prospects," *NDT & E International*, vol. 142, p. 103026, 2024, doi: 10.1016/j.ndteint.2023.103026.

[2] K.-Y. Jhang, "Nonlinear ultrasonic techniques for nondestructive assessment of micro damage in material: A review," *Int. J. Precis. Eng. Manuf.*, vol. 10, no. 1, pp. 123–135, 2009, doi: 10.1007/s12541-009-0019-y.

[3] S. Palitsagar, S. Das, N. Parida, and D. Bhattacharya, "Non-linear ultrasonic technique to assess fatigue damage in structural steel," *Scripta Materialia*, vol. 55, no. 2, pp. 199–202, 2006, doi: 10.1016/j.scriptamat.2006.03.037.

[4] K. H. Matlack, J.-Y. Kim, L. J. Jacobs, and J. Qu, "Review of second harmonic generation measurement techniques for material state determination in metals," *J Nondestruct Eval*, vol. 34, no. 1, 2015, doi: 10.1007/s10921-014-0273-5.

[5] N. J. Carino, "The Impact-Echo Method: An overview," in *Proceedings of the 2001 Structures Congress & Exposition*, American Society of Civil Engineers, Ed., 2001, pp. 1–18.

[6] A. J. Croxford, P. D. Wilcox, B. W. Drinkwater, and P. B. Nagy, "The use of non-collinear mixing for nonlinear ultrasonic detection of plasticity and fatigue," *The Journal of the Acoustical Society of America*, vol. 126, no. 5, EL117-22, 2009, doi: 10.1121/1.3231451.

[7] Y. Wang and J. D. Achenbach, "Reflection of ultrasound from a region of cubic material nonlinearity due to harmonic generation," *Acta Mech*, vol. 229, no. 2, pp. 763–778, 2018, doi: 10.1007/s00707-017-1996-z.

[8] M. Hasanian and C. J. Lissenden, "Second order harmonic guided wave mutual interactions in plate: Vector analysis, numerical simulation, and experimental results," *Journal of Applied Physics*, vol. 122, no. 8, 2017, Art. no. 084901, doi: 10.1063/1.4993924.

[9] M. Hasanian and C. J. Lissenden, "Second order ultrasonic guided wave mutual interactions in plate: Arbitrary angles, internal resonance, and finite interaction region," *Journal of Applied Physics*, vol. 124, no. 16, 2018, Art. no. 164904, doi: 10.1063/1.5048227.

[10] Y. Wang and J. D. Achenbach, "Interesting effects in harmonic generation by plane elastic waves," *Acta Mech. Sin.*, vol. 33, no. 4, pp. 754–762, 2017, doi: 10.1007/s10409-017-0676-5.

[11] V. E. Nazarov and A. M. Sutin, "Nonlinear elastic constants of solids with cracks," *The Journal of the Acoustical Society of America*, vol. 102, no. 6, pp. 3349–3354, 1997, doi: 10.1121/1.419577.

[12] J. L. Rose, *Ultrasonic Guided Waves in Solid Media*. Cambridge University Press, 2014.

[13] V. A. Korneev and A. Demčenko, "Possible second-order nonlinear interactions of plane waves in an elastic solid," *The Journal of the Acoustical Society of America*, vol. 135, no. 2, pp. 591–598, 2014, doi: 10.1121/1.4861241.

[14] W. de Lima and M. F. Hamilton, "Finite-amplitude waves in isotropic elastic plates," *Journal of Sound and Vibration*, vol. 265, no. 4, pp. 819–839, 2003, doi: 10.1016/S0022-460X(02)01260-9.

[15] J. Vidler, A. Kotousov, and C.-T. Ng, "Development of Micro-mechanical Models of Fatigue Damage," in *Proceedings of the Third International Conference on Theoretical, Applied and Experimental Mechanics*, (n.d.), pp. 145–150.